11th Nordic Symposium on Building Physics, NSB2017, 11-14 June 2017, Trondheim, Norway

Characterization of the thermal structure of different building constructions using in-situ measurements and Bayesian analysis

Virginia Gori [a],*, Clifford A. Elwell[a]

a UCL Energy Institute, 14 Upper Woburn Street, London WC1E 6BT, United Kingdom

Abstract

A dynamic method, comprising a two lumped-thermal-mass model and Markov Chain Monte Carlo sampler, was used to analyze in-situ-monitored data and estimate the thermophysical properties of two walls of different construction. This method, unlike maximum a posteriori approaches, estimates the parameters' probability distributions, providing insight into the wall's thermal structure.

Total R-values were well defined for both walls, whilst constituent estimated R-values for a solid wall having layers of materials with similar thermal properties were anticorrelated (thermal mass locations weakly constrained), but were not correlated for an insulated cavity wall with thermally distinct layers (thermal mass locations strongly thermally constrained).

© 2017 The Authors. Published by Elsevier Ltd.
Peer-review under responsibility of the organizing committee of the 11th Nordic Symposium on Building Physics.

Keywords: Heat transfer; In-situ measurements; U-value; R-value; Thermal mass; External wall; Bayesian statistics; MCMC; Grey-box model

1. Introduction

Evaluating the energy performance of buildings is key to reduce energy demand and carbon emissions of the built environment [1] and to achieve climate change mitigation targets [2-5]. Understanding the thermophysical structure and behavior of the building envelope is fundamental to inform targeted policy-making strategies; to ensure quality assurance of new constructions; and to inform the decision-making process prior to retrofitting interventions to deliver tailored and cost-effective solutions that aim to reduce energy consumption while maximizing the thermal comfort [6].

---

* Corresponding author. Tel.: +44 203 108 9830.
   E-mail address: virginia.gori.12@ucl.ac.uk

In principle, the thermal properties (*e.g.*, R-value and thermal mass) of a building element can be easily estimated knowing the thickness and the tabulated thermal properties (*e.g.*, thermal conductivity, density and specific heat capacity) of the materials it is made of [7]. However, several studies [8-10] have shown discrepancies between the performance expected from lookup tables and that estimated from in-situ measurements – a phenomenon known as performance gap [8].

Thermophysical properties evaluated from tabulated values often present a number of uncertainties as only visual inspection or quick surveys of the element under study is common [11]. Literature values for a given material may present quite broad ranges, and materials with similar appearance may have quite different thermophysical behavior [7]. Environmental conditions, structural and situational inhomogeneities (*e.g.*, cracks, gaps, moisture accumulation) [11] – which are not accounted for in tabulated values – may also influence the as-built performance of building elements and contribute towards the performance gap. The use of monitored data (*i.e.* heat flux and temperatures) overcomes these limitations as they account for the local environmental conditions the element is exposed to and its state of conservation [12], and do not require any knowledge of the stratigraphy under study.

This paper uses the dynamic grey-box method presented by Gori et al. [6,13] to estimate the thermophysical properties of two walls of different construction. The method consists of a combination of a two lumped-thermal-mass model (used to describe the heat transfer across the element) and Bayesian-based optimization techniques with a Markov Chain Monte Carlo (MCMC) sampler (used to estimate the best set of parameters and the associated errors). Unlike the maximum a posteriori (MAP) approach, the MCMC framework also allows the full estimation of the probability distributions of the parameters of the model instead of just their most probable value. Additionally, the statistical framework enables the characterization of the errors on the estimates and the potential correlation among them.

Practical advantages of the use of monitored data and the statistical framework include its suitability for any type of building (including historical ones) as it is non-destructive and does not require any knowledge of the stratigraphy of the element investigated. This enables the identification of retrofitting strategies that maximize thermal comfort and minimize energy use through customized insulation, heating and cooling strategies. This paper explores the potential applicability of this method to complement in-situ surveys and provide additional insight into the thermal structure of building elements using relatively cheap and non-destructive techniques (*e.g.*, to identify whether the element is likely to have been already insulated).

Nomenclature

|	
R_n	n-th lumped thermal resistance (starting from the internal side) $[\text{m}^2\text{KW}^{-1}]$
C_n	n-th lumped thermal mass (starting from the internal side) $[\text{Jm}^{-2}\text{K}^{-1}]$
$T_{C_n}^0$	Initial temperature of the n-th lumped thermal mass (starting from the internal side) $[^\circ\text{C}]$
$Q_{\text{m,in}}$	Measured heat flux entering the internal surface of the wall $[\text{Wm}^{-2}]$
$Q_{\text{m,out}}$	Measured heat flux leaving the external surface of the wall $[\text{Wm}^{-2}]$
T_{int}	Measured temperature on the internal surface of the wall $[^\circ\text{C}]$
T_{ext}	Measured temperature on the external surface of the wall $[^\circ\text{C}]$
$\boldsymbol{\theta}$	Vector of parameters of the model
$\boldsymbol{\theta}_{\text{2TM}}$	Vector of the best-fit parameters of the model
D	Measured data
H	Model
$P(\boldsymbol{\theta}|D,H)$	Posterior distribution
$P(D|\boldsymbol{\theta},H)$	Likelihood
$P(\boldsymbol{\theta}|H)$	Prior distribution
$P(D|H)$	Evidence
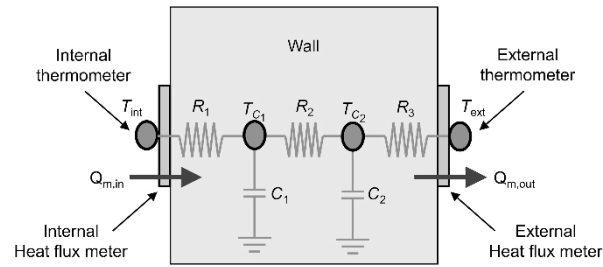
Fig. 1 Schematic of the two-thermal-mass (2TM) model showing the equivalent electric circuit, the measured quantities and the seven parameters of the model.

2. Case studies and monitoring campaign

Two walls of different construction were investigated. The first wall, OWall, of solid-brick masonry was north-west-facing and located on the first floor above ground of an office building in London (UK). From indoors, it consisted of 20±5 mm of plaster and 350±5 mm of exposed solid brick masonry for a total thickness of 370±7 mm.

The second wall, HWall, was a north-facing cavity wall located on the ground floor of a 1970s occupied house in Cambridgeshire (UK). From the inside, it comprised 10±5 mm of plaster, 100±5 mm aerated concrete blocks, a 65±5 mm thick cavity filled with urea formaldehyde foam and 100±5 mm of bricks. The total thickness was 275±10 mm. Visual inspection suggested significant shrinkage of the original full fill of insulation.

Both case studies were instrumented using two Hukseflux HP01 [14] heat flux plates (HFP) and two thermistors, each placed on opposite sides of the wall and in-line with each other. Data were averaged over 5 minute intervals using a Campbell Scientific 1000 [15] logger for the OWall and an Eltek Squirrel 451/L [16] for the HWall.

3. Theory and calculation

3.1. The grey-box dynamic method

The thermophysical structure of each case study was investigated by means of a grey-box dynamic method (comprehensively described in [6,13]) using a two lumped-thermal-mass (2TM) model to describe the heat transfer across the building element and Bayesian-based optimization techniques with an MCMC sampler to estimate the best set of parameters of the model, their distributions and their associated errors.

The 2TM model (Fig. 1) includes seven parameters, namely: three thermal resistances (R_n), two effective thermal masses (C_n), and their initial temperature $\left(T_{C_n}^0\right)$. Measured quantities are the heat fluxes through the internal and external surfaces of the wall and the surface temperatures. From Bayes' rule [17], the best-fit parameters $(\boldsymbol{\theta}_{2\text{TM}})$ can be estimated by maximizing the posterior probability $(P(\boldsymbol{\theta}|D,H))$ as:

$$\boldsymbol{\theta}_{2\text{TM}} = \arg\max_\theta \text{P}(\boldsymbol{\theta}|D,H) = \arg\max_\theta \frac{\text{P}(D|\boldsymbol{\theta},H)\text{P}(\boldsymbol{\theta}|H)}{\text{P}(D|H)} \tag{1}$$

where $\text{P}(D|\boldsymbol{\theta},H)$ is the likelihood (*i.e.* a data-dependent term describing the probability of obtaining the measured data, D, given the model, H, and the parameters, $\boldsymbol{\theta}$), $\text{P}(\boldsymbol{\theta}|H)$ is the prior probability (*i.e.* an initial probability distribution of the parameters of the model according to previous knowledge), and $\text{P}(D|H)$ is the evidence (*i.e.* a normalization factor). The likelihood was calculated from the residuals between the measured and estimated internal and external heat fluxes, where the assumption of independent and identically distributed (i.i.d.) Gaussian observation errors was relaxed by introducing a prior on the residuals to account for their potential autocorrelation [13].

An MCMC sampler was used to estimate the best-set of parameters and their probability distributions. Unlike maximum a posteriori (MAP) approaches, where only the best-set of parameters is estimated, the MCMC framework
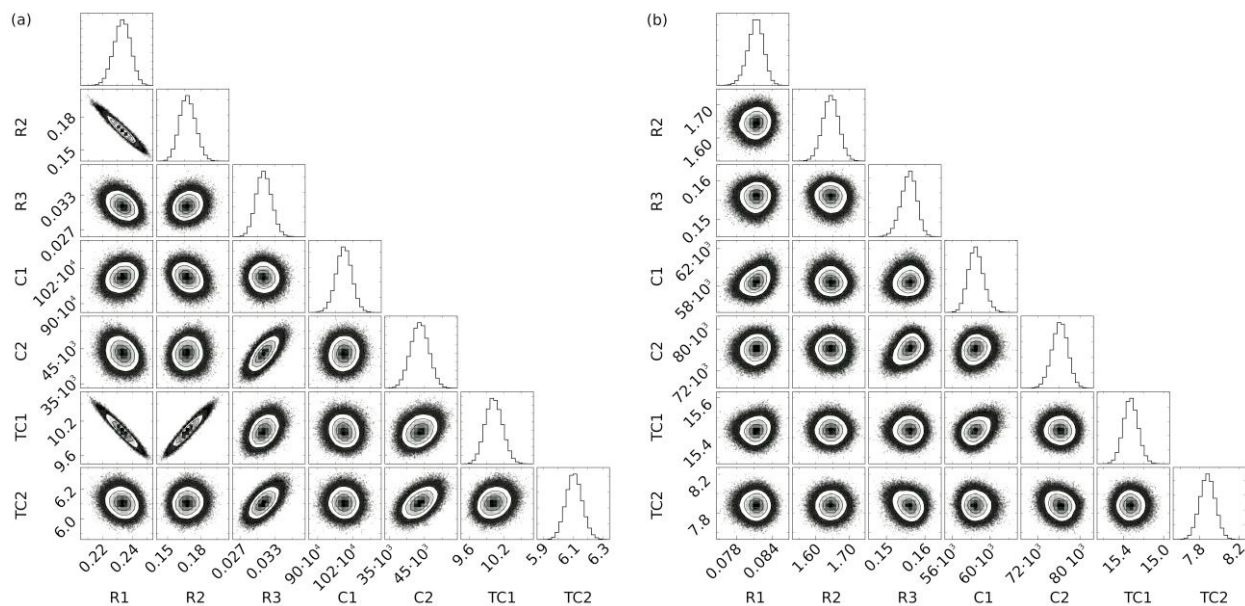
Fig. 2 Distribution of the estimates of the thermophysical parameters for the OWall (a) and the HWall (b); the estimates for the first of the four monitored periods are shown.

gives additional information on the shape and the distribution of the parameters. The framework was implemented in Python and used the EMCEE library [18] for the MCMC sampling [13].

3.2. Prior probability distribution on the parameters of the model

Large uniform priors on the parameters of the model were used in this application as the lack of information about the distribution of the thermophysical properties for some of the materials constituting the case studies prevented the implementation of more informative non-uniform priors (*e.g.*, log-normal distributed as in [13]).
Priors on all thermal resistances were set to the same range of 0 to 4 m^2KW^{-1}; all effective thermal masses 0 to $2 \cdot 10^6$ $Jm^{-2}K^{-1}$ and initial temperatures of the effective thermal masses from -5 to 30 °C. These ranges encompass all expected values, with significant safety margin.

4. Results and discussion

The estimates of the thermophysical properties of the two case studies (OWall and HWall) are presented below. For each case study, four periods were selected from a longer monitoring campaign (respectively undertaken in winter 2013/2014 and winter 2016) by imposing the criteria described in Section 7.1 of the BS ISO 9869-1 Standard [19] to ensure that the time series analyzed had stabilized. More than one monitoring period was analyzed for each case study to ensure that the observed behavior was typical. In the following, only the first period is described in detail (Fig. 2), while the others are summarized in Fig. 3.

To facilitate comparison of the estimates, the mean of the parameter distribution was calculated. The total R-value (and U-value) was calculated as the sum of R_n in the model, plus a correction factor that accounts for the internal (0.13 m^2KW^{-1}) and external (0.04 m^2KW^{-1}) air film resistances and removes the thermal resistance of the HFPs ($6.25 \cdot 10^{-3}$ m^2KW^{-1}). Detailed error analysis was performed following [13]. Only the systematic error on the U-value (*i.e.* the error due to biases in the monitoring equipment or to unmodelled physical processes) is reported as it dominates errors, whilst the statistical error (*i.e.* the error due to the data-fitting process) was smaller by an order of

magnitude in all cases. The statistical errors output by the Bayesian analysis are reported for the total R-value and effective thermal mass estimates.
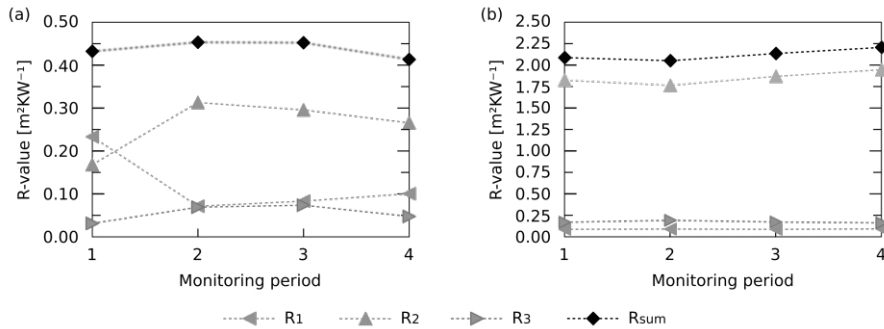

Fig. 3 Estimates of the lumped thermal resistances and their sum for the four monitoring periods, respectively for the OWall (a) and HWall (b).

The total R-value for the OWall (calculated from the mean of the distributions in Fig. 2) was 0.59 ± 0.01 m^{2}KW^{-1}, resulting in a U-value of 1.66 ± 0.15 Wm^{-2}K^{-1}. The effective internal and external thermal masses were respectively $(9.90\pm0.27)\cdot10^5$ Jm^{-2}K^{-1} and $(0.44\pm0.03)\cdot10^5$ Jm^{-2}K^{-1}. Similarly, for the HWall the total R-value was 2.04 ± 0.02 m^{2}KW^{-1} and the U-value 0.49 ± 0.04 Wm^{-2}K^{-1}. The effective internal and external thermal masses were respectively (5.85 ± 0.08) 10^4 Jm^{-2}K^{-1} and (7.62 ± 0.15) 10^4 Jm^{-2}K^{-1}.

Fig. 2 shows the distribution of the thermophysical parameters, for both the OWall and HWall. The histograms along the diagonal show the marginalized distribution for each parameter, while the other panels represent the marginalized 2D distributions for each pair of parameters. This type of graph provides useful information about the correlation between parameters of the model, which can be used to gain insights into the thermal structure of the wall and, for example, to inform the decision-making process. When a pair of parameters is uncorrelated, the posterior probability is often circular or elliptical with axes parallel to the Cartesian axes. Conversely, when the pair of parameters is correlated, the posterior probability distribution is rotated, and the orientation of the major axis of the ellipsis indicates the nature of the relationship (positive or negative). Fig. 2(a) shows a negative correlation among the thermal resistance estimates, suggesting that the total R-value of the wall – and consequently its U-value – was constant but the relative magnitude of the individual lumped thermal resistances may vary (*e.g.*, an increase in R_1 tends to be compensated by a decrease in R_2). Conversely, no correlation is shown among the thermal resistances of the HWall (Fig. 2(b)), suggesting that the model finds these thermal resistances to be independent of each other.

The results obtained in Fig. 2 were confirmed by the additional three periods analyzed (Fig. 3). As expected, for the OWall (Fig. 3(a)), the sum of the individual R-value estimates is almost constant across the four monitoring periods, whilst the magnitude of the constituent R-values varies. Conversely, for the HWall (Fig. 3(b)), both the sum and the individual R-value estimates are relatively stable across the different periods surveyed.

The model results suggest that when the materials constituting a building element have very distinct thermophysical properties, like a filled cavity wall (with a high thermal resistance and low thermal mass material interposed between two layers of lower thermal resistance), the position of the effective thermal masses is well defined. The effective thermal masses are located within the masonry layers whilst the insulation between them imposes a strong physical constraint, and consequently a unique solution to the values of the constituent thermal masses in the model (R_n). Conversely, when the thermophysical properties of the layers constituting the element are comparable, like in a traditional solid wall, the weak physical constraints allow several similarly probable combinations for the locations of the effective lumped thermal masses. Consequently, the size of the constituent thermal resistances (R_n) will vary depending on the effective thermal mass position, but their total R-value is constant.

5. Conclusions

This paper explores the use of a dynamic grey-box method to provide insight into the thermal structure of building elements, which can be used to support building surveys and inform tailored retrofitting strategies. The method,

consisting of a two lumped-thermal-mass model and an MCMC sampler, was used to analyze in-situ measurements of two walls of different construction and estimate their thermophysical properties. Unlike the MAP approach, the MCMC framework not only provides the best-estimate of the thermophysical parameters of the model but also their distribution.

The distribution of the parameters provided useful insight into the thermal structure of the elements investigated, which can be interpreted in the light of the building stratigraphy. Whilst the topic of future work, potential practical applications of this framework include its use as a tool to support non-destructive in-situ surveys and to inform the decision-making process, for example: to identify the most probable materials constituting a building element; to evaluate whether a building structure is likely to be insulated; and to propose tailored retrofitting strategies aiming at maximizing the thermal comfort within the indoor ambient and the thermal performance of the building, while minimizing the overall energy consumption.

Acknowledgements

References

[1] International Energy Agency. Transition to Sustainable Buildings Strategies and Opportunities to 2050. *Tech. Rep.* 2013.

[2] European Community. The EU Climate and Energy Package. 2009.

[3] European Community. A roadmap for moving to low-carbon economy in 2050. 2010.

[4] Climate Change Act. C. 27. 2008.

[5] Department of Energy and Climate Change. The UK Low Carbon Transition Plan – National strategy for climate and energy. 2009.

[6] Gori V, Marincioni V, Biddulph P, Elwell CA. Inferring the thermal resistance and effective thermal mass distribution of a wall from in situ measurements to characterise heat transfer at both the interior and exterior surfaces. *Energy Build.* 2017;135:398-409.

[7] Chartered Institution of Building Services Engineers (CIBSE). Guide A: Environmental design. 7th rev. Norwich, UK: Page Bros. Ltd; 2007.

[8] Zero Carbon Hub. Closing the gap between design & as-built performance, End of term report. *Tech. Rep.* 2014.

[9] Li FGN, Smith AZP, Biddulph P, Hamilton IG, Lowe R, Mavrogianni A, Oikonomou E, Raslan R, Stamp S, Stone A, Summerfield A, Veitch D, Gori V, Oreszczyn T. Solid-wall U-values: heat flux measurements compared with standard assumptions. *Build Res Inf.* 2014;43:238–252.

[10] Xeni, F, Eleftheriou P, Michaelides I, Hadjiyiannis S, Philimis P, Stylianou A. In situ U-value measurements for today's Cypriot houses. *Int J Sustain Energ.* 2015; 34(3-4):248-258.

[11] Biddulph P, Gori V, Elwell CA, Scott C, Rye C, Lowe R, Oreszczyn T. Inferring the thermal resistance and effective thermal mass of a wall using frequent temperature and heat flux measurements. *Energy Build.* 2014;78:10-16.

[12] Cesaratto PG, De Carli M. A measuring campaign of thermal conductance in situ and possible impacts on net energy demand in buildings. *Energy Build.* 2013;59;29-36.

[13] Gori V. A novel method for the estimation of thermophysical properties of walls from short and seasonal-independent in-situ surveys, PhD. UCL, London, UK. 2017 (in press).

[14] Hukseflux. HFP01 Heat flux plate [online]. 2015.

[15] Campbell Scientific. CR1000 Measurement and control datalogger [online]. 2015.

[16] Eltek. Squirrel 450/850 series data logger [online]. 2015.

[17] MacKay DJ. Information theory, inference, and learning algorithms. 4th ed. Cambridge, UK: Cambridge University press; 2003.

[18] Foreman-Mackey D, Hogg DW, Lang D, Goodman J. emcee: The MCMC Hammer. *Publ Astron Soc Pac.* 2013;125(925):306-312.

[19] BS ISO 9869-1. Thermal insulation – Building elements – *In-situ* measurements of thermal resistance and thermal transmittance. Part1: Heat flow meter method. 2014.